SSC23-VI-01

Extended Life Qualification of the Magnetically Shielded Miniature (MaSMi) Hall Thruster

Vernon H. Chaplin, Jacob B. Simmonds, Matthew P. Byrne, Dan M. Goebel, Alejandro Lopez Ortega, Robert B. Lobbia, Ioannis G. Mikellides, Richard R. Hofer, Brian X. Zhu, John M. Ratliff
Jet Propulsion Laboratory, California Institute of Technology
4800 Oak Grove Dr., Pasadena, CA 91109; 818-393-8203; vernon.h.chaplin@jpl.nasa.gov

Ryan W. Conversano
Exoterra Resource, LLC
7640 S. Alkire Place, Littleton, CO 82127

ABSTRACT

We present an update on the life qualification of the Magnetically Shielded Miniature (MaSMi) Hall thruster (also known as the ASTRAEUS Thruster Element), which was developed at the Jet Propulsion Laboratory and was recently licensed to ExoTerra Resource for flight production (renamed Halo12). In 2020–2021, the thruster successfully completed a 7205-hour wear test at operating powers from 200–1350 W, processing over 100 kg of xenon propellant and producing 1.55 MN-s total impulse with no measurable degradation in performance. The wear test is being extended to further demonstrate the service life capability of the thruster. In separate tests, proto-flight MaSMi hollow cathodes demonstrated >25000 ignition cycles and >13000 hours of operation at 4 A discharge current, and a set of three MaSMi electromagnets underwent >3000 deep thermal cycles (-123 °C to 495 °C). Laser-induced fluorescence (LIF) measurements of ion velocities and plasma modeling with Hall2De, a widely published numerical plasma code, have been carried out to elucidate the physical mechanisms driving pole erosion trends observed in thruster wear testing. Survival probabilities for micrometeoroid impacts and other random failure modes in flight were also analyzed.

INTRODUCTION

The Magnetically Shielded Miniature (MaSMi) Hall thruster was developed at the Jet Propulsion Laboratory (JPL) and the University of California, Los Angeles (UCLA) from 2011–2021[1–9] to provide a high-performance,[7] long-life[10,11] propulsion capability for interplanetary small satellite missions requiring high Δv. Key features include magnetic shielding to effectively eliminate channel wall erosion,[12–14] a design optimized for efficiency across a wide throttling range using advanced plasma modeling tools,[2–4] and a heaterless lanthanum hexaboride (LaB_6) hollow cathode[15–19] that is centrally mounted to minimize the thruster's susceptibility to facility effects.[20]

The MaSMi thruster technology was recently licensed to ExoTerra Resource, LLC for flight production, where it was renamed Halo12 and will be paired with an Exoterra-developed power processing unit (PPU) and xenon flow controller (XFC). Flight qualification[21] of the thruster began at JPL in 2019. The qualification testing has included a 7205-hour wear test during which the thruster processed > 100 kg of xenon propellant and produced 1.55 MN-s total impulse,[11] a >3000-cycle thermal vacuum (TVAC) test of the inner coils from -123 °C to 495 °C,[22] and two stand-alone cathode tests demonstrating >25000 heaterless ignitions[19] and >13,000 hours of operation at 4 A discharge current,[10] respectively. All of these tests were voluntarily terminated due to programmatic constraints while the test articles were still operational. Qualification-level vibration and shock tests were successfully carried out on a MaSMi-EM (Engineering Model) unit at JPL, and an upcoming full-thruster TVAC test at Exoterra will satisfy the final requirement to reach NASA Technology Readiness Level (TRL) 6, defined as a "system or subsystem prototype demonstration in a relevant environment".[23]

This paper describes the status of additional ongoing activities at JPL to extend the life qualification of the thruster and demonstrate its readiness for flight. The second section summarizes the thruster wear test results to date, describes follow-on studies being pursued to understand the erosion trends observed in the wear test, and lays out the goals for

the wear test extension. The third section provides an update on the cathode life assessment, focusing on new erosion modeling results obtained with the OrCa2D[24] plasma code. The fourth section describes reliability analyses carried out to quantify the random failure risk in flight, including a calculation of the failure rate due to micrometeoroid impacts. Conclusions are provided in the final section.

THRUSTER WEAR TESTING

The original Long Duration Wear Test (LDWT) of a MaSMi-EM thruster (also called the thruster element of JPL's Ascendant Transcelestial Electric Propulsion System - ASTRAEUS) at JPL consisted of 7205 total hours of thruster operation at five operating conditions spanning discharge voltages from 200–500 V and discharge powers from 200–1350 W. Results of the test are described in detail in Ref. 11. Thrust performance at the five conditions was measured periodically and was found to be invariant over the duration of the test, with total efficiency reaching 60% at the 300 V/1350 W operating condition. Plume probe data were also collected periodically, and temperatures at eight locations on the thruster were monitored. Optical profilometry was used between each test segment to measure the accumulated erosion of the graphite front pole covers, which is the dominant life-limiting erosion process in magnetically shielded Hall thrusters since channel erosion is negligible.

Long Duration Wear Test Extension

The MaSMI-EM LDWT will be extended with the same test article to further demonstrate the life capability of the thruster. The test plan calls for a series of 250–300 hour test segments at operating conditions within the previously demonstrated 200-500 V and 200–1350 W throttling envelope, with erosion rates characterized via profilometry between each segment. Calibrated thrust measurements and plume probe measurements including Faraday probe (ion current density), ExB probe (ion charge state fractions), retarding potential analyzer (distribution of ion energy per charge), and Langmuir probe (electron temperature, electron density, and plasma potential) will be made at least once per segment. Basic electrical telemetry and discharge oscillation statistics will be recorded continuously throughout the automated test. As discussed in the following section, the thruster face eroded asymmetrically during the original LDWT—in order to gather additional information about the root cause of this phenomenon, the mounting orientation of the thruster will be rotated for the LDWT Extension to allow the plume probe array to sweep horizontally across the plane containing the maximum- and minimum-erosion locations. After making this rotation, any change in the azimuthal location of peak erosion going forward may point to facility interactions as a contributing factor.

Investigation of Pole Erosion Trends in MaSMi-EM

The MaSMi-EM wear test thruster was still performing nominally after the initial 1.55 MN-s LDWT, and it is expected to have significant additional life remaining.[11] However, the measured erosion rates of the front pole covers, particularly on the outer side of the channel, were higher than expected based on previous testing[5] and modeling[4] of a MaSMi Development Model (DM) thruster that had a nearly identical design magnetic field topology and plasma-facing geometry, and unexpected azimuthal asymmetry was observed. Measured erosion rates from the first two segments of the EM wear test (spanning >5000 hours of thruster operation) are shown in Figs. 1 and 2. The radial peak of the azimuthally-averaged outer pole cover erosion rate is ~ 350 μm/kh at both operating conditions, with higher erosion rates on one side of the thruster. For comparison, MaSMi-DM erosion rates during short duration wear tests at 500 V/1000 W and 400 V/800 W were < 30 μm/kh on the inner pole cover and < 20 μm/kh on the outer pole cover.[5]

Investigations are ongoing to understand the cause of these erosion trends in the EM wear test thruster. High-resolution magnetic field mapping has been carried out, along with anode flow uniformity checks and CT scanning. An extensive campaign of laser-induced fluorescence (LIF)[25] measurements was recently completed to compare the ion velocities on the high- and low-erosion sides of the thruster, characterize the dependence of the ion acceleration region location on variables such as the facility background pressure and the thruster's magnetic field strength, and make comparisons with previous LIF measurements on MaSMi-DM.[6]

LIF involves injection of a laser beam into the plasma to excite a bound electron transition within an ion or atom, followed by detection of the photon emitted when the electron falls back down to a lower energy state. The laser photon can only be absorbed by the ion if its wavelength in the ion's rest frame is equal to the transition wavelength λ^*. For ions moving along the laser injection direction,

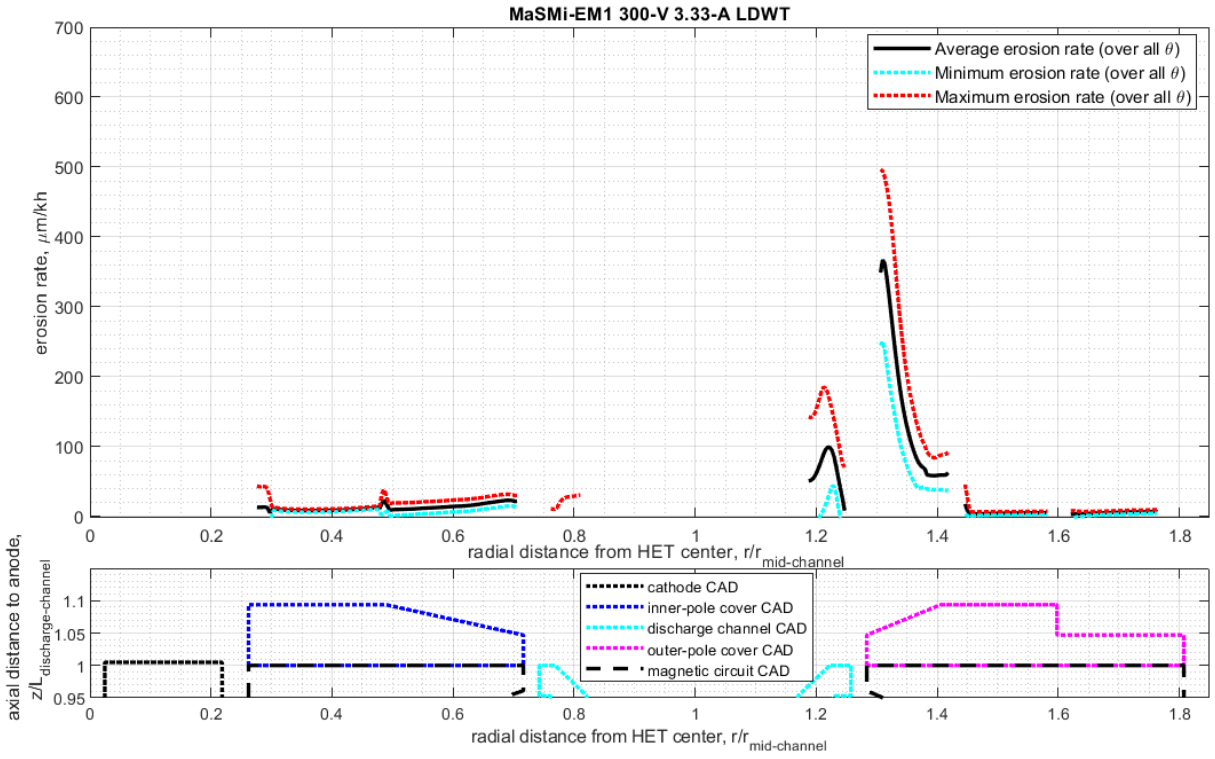

Figure 1: Erosion rates across the inner and outer pole cover faces measured during the previous MaSMi-EM LDWT at the 300 V/1000 W operating condition. Rates at the azimuthal locations of maximum and minimum erosion are shown, along with the azimuthal average.

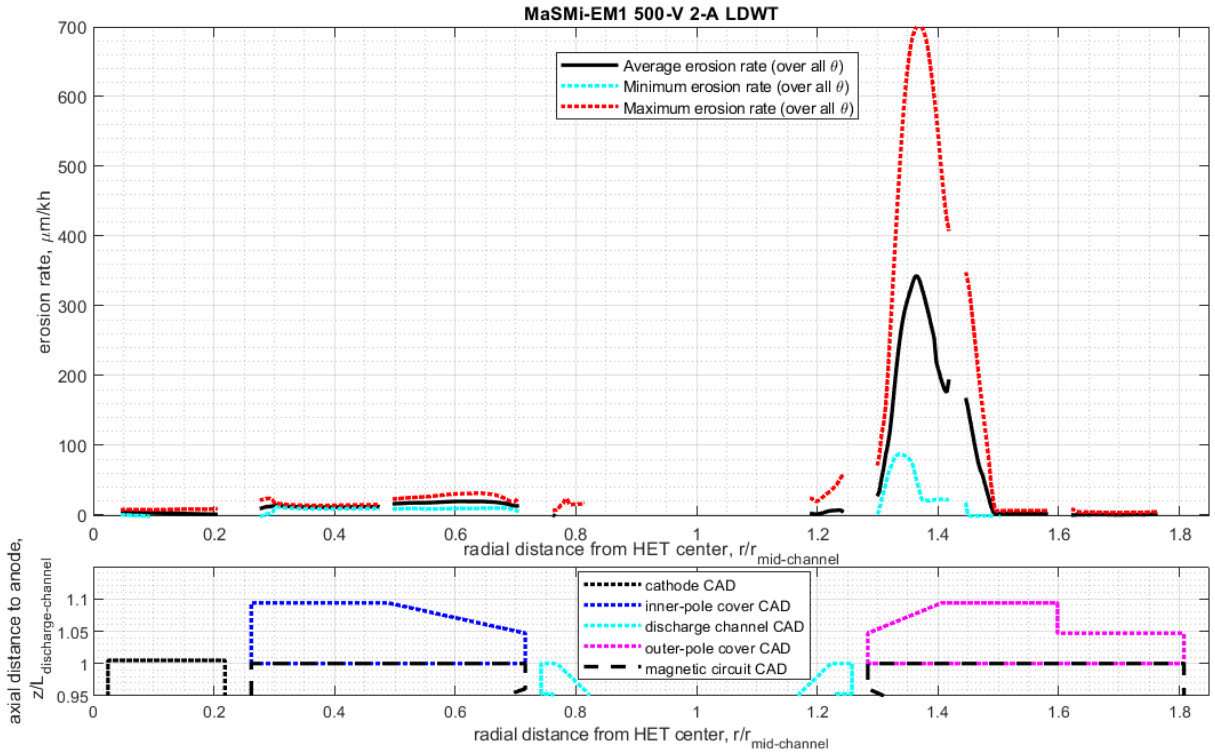

Figure 2: Same as Fig. 1, for the 500 V/1000 W operating condition.

the photon wavelength seen by the ion is Doppler shifted:

$$\lambda_{ion\ frame} = \frac{\lambda_{lab\ frame}}{1 + v_{ion}/c}, \quad (1)$$

where c is the speed of light. The fluorescence signal detected at a given laser wavelength $\lambda_{lab\ frame}$ is proportional to the density of ions with the velocity v_{ion} needed to make $\lambda_{ion\ frame} = \lambda^*$. Thus by scanning the laser through a range of wavelengths, it is possible to map out the local ion velocity distribution function $f_i(v)$. The mean ion velocity along a given direction can be calculated from the first moment of the 1D distribution function; for example, $u_z = \int v_z f_i(v_z)\, dv_z$.

In the setup for the MaSMi-EM measurements, laser beams were injected along two orthogonal directions 45 degrees offset from the axial and radial directions. The measurement volume remained fixed in space, and the thruster was translated on a two-axis motion stage assembly to allow measurements to be made at different locations in the thruster coordinate system (see Fig. 1 of Ref. 26 for an example of a similar setup). All measurements were made in the vertical midplane of the thruster, which was mounted at a 45-degree angle with respect to its original configuration for the wear test so that the LIF measurement plane spanned the azimuthal locations with the highest and lowest outer pole erosion (see Fig. 3).

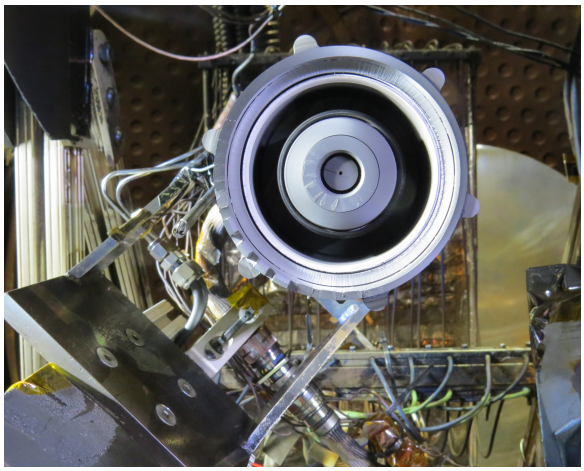

Figure 3: MaSMi-EM wear test thruster mounted for the LIF test such that the azimuthal locations with the highest and lowest outer pole erosion were at the 3:00 and 9:00 positions, respectively.

LIF data were acquired at the five operating conditions from the LDWT, at the locations shown in Fig. 4 (some locations were not studied at every operating condition). The majority of the data points were acquired on the side of the thruster with higher outer pole cover erosion. In order to look for asymmetry in the ion velocities that could be correlated with the erosion asymmery, a subset of the points were repeated on the low erosion side, focusing on locations near the outer pole and regions of the channel around the acceleration region.

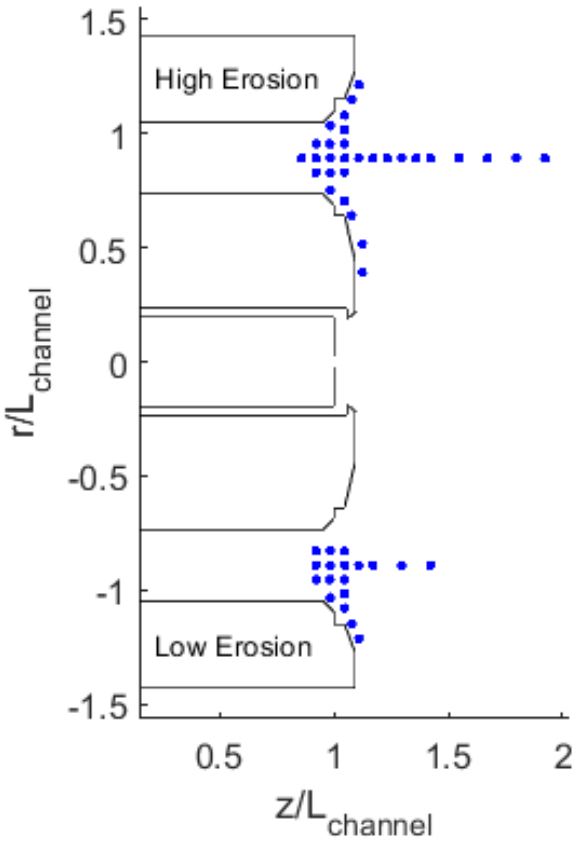

Figure 4: LIF measurement locations for the investigation of pole erosion trends in the MaSMi-EM wear test thruster.

Figure 5 shows examples of measured ion velocity distributions functions in front of the outer and inner poles for the highest power (300 V/1350 W) LDWT operating condition. The Axis 1 data (blue curve) in front of the outer pole features a sharp high-velocity peak corresponding to fast ions accelerated radially from the edge of the beam, and a low-energy tail corresponding to ions born below the anode potential. The measured ion velocities along Axis 2 (red curve) are mostly close to zero, indicating that the majority of both the fast and slow ions were moving approximately along Axis 1 (with comparable positive axial and radial velocity components). In front of the inner pole, the presence of two velocity peaks along both measurement axes likely indicates

the presence of two counter-streaming ion populations, one originating from the channel region and the other from the cathode plume. A similar phenomenon has been observed in a larger magnetically shielded Hall thruster.[27]

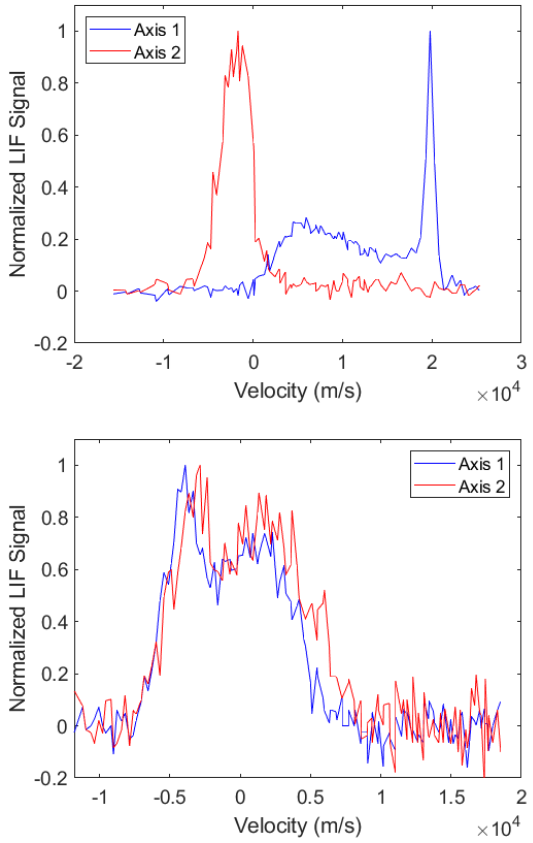

Figure 5: Ion velocity distribution functions along the two 45-degree diagonal LIF measurement axes (positive velocities along Axis 1 are radially outward and positive velocities along Axis 2 are radially inward) for points in front of the outer pole at $z/L_{channel} = 1.11$, $r/L_{channel} = 1.21$ (top panel) and in front of the inner pole at $z/L_{channel} = 1.13$, $r/L_{channel} = 0.39$ (bottom panel) at the 300 V/1350 W operating condition.

High-fidelity physics-based modeling with the Hall2De code[28] has shown that the front poles erode in magnetically shielded thrusters in part because the acceleration region is located further downstream than in unshielded thrusters, at or beyond the channel exit, which allows trajectories of beam-edge ions born near the anode potential to intersect the poles.[29] Small axial shifts in the acceleration region position (<5% of the channel length), which depends on non-classical cross-field electron transport[30,31] and thus cannot currently be predicted from first principles,[32] have been shown to produce large changes in the outer pole erosion rate in simulations. Therefore, a significant portion of the LIF campaign on the wear test thruster was dedicated to comparing the acceleration region location in different scenarios potentially relevant to the erosion trends.

In particular, one goal was to compare ion velocities measured in the EM thruster with those measured previously in the DM.[6] Results are shown for the 500 V/1000 W operating condition in Fig. 6. A pumping system upgrade prior to the EM testing lowered the achievable facility background pressure, which can affect the acceleration zone location,[26,33] so a second LIF dataset was acquired for the EM with the background pressure increased by auxiliary xenon injection at the far end of the chamber.[13] All three ion acceleration profiles were identical to within the LIF alignment uncertainty, ruling out an acceleration region shift as a significant contributor to the EM versus DM erosion differences at this condition. Additional results from the LIF measurements on the EM wear test thruster will be presented in a future publication.

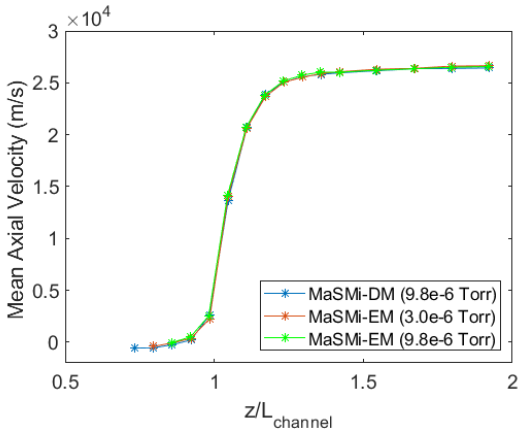

Figure 6: Measured ion acceleration profile along the channel centerline at 500 V/1000 W in the MaSMi-DM thruster and on the high-erosion side of the MaSMi-EM wear test thruster at two different background pressures.

CATHODE LIFE ASSESSMENT

Previous Cathode Qualification Testing

MaSMi's compact heaterless hollow cathode previously underwent a 13-kh life test at 4 A discharge

current.[10] Cathode performance as measured by the discharge voltage and keeper floating voltage did not change significantly over the course of the test, and the quantity of LaB_6 emitter material remaining when the cathode was cross-sectioned after voluntary termination of the test suggested that only $\sim 1/2$ of the emitter life had been expended. In a separate test,[19] a MaSMi-EM cathode completed >25000 rapid ignition cycles with no significant degradation in steady-state operating characteristics; the ignition time was $\ll 1$ s for the first > 10000 cycles, far more than would be required in practical mission applications, and heaterless ignitions were still possible after 25000 cycles.

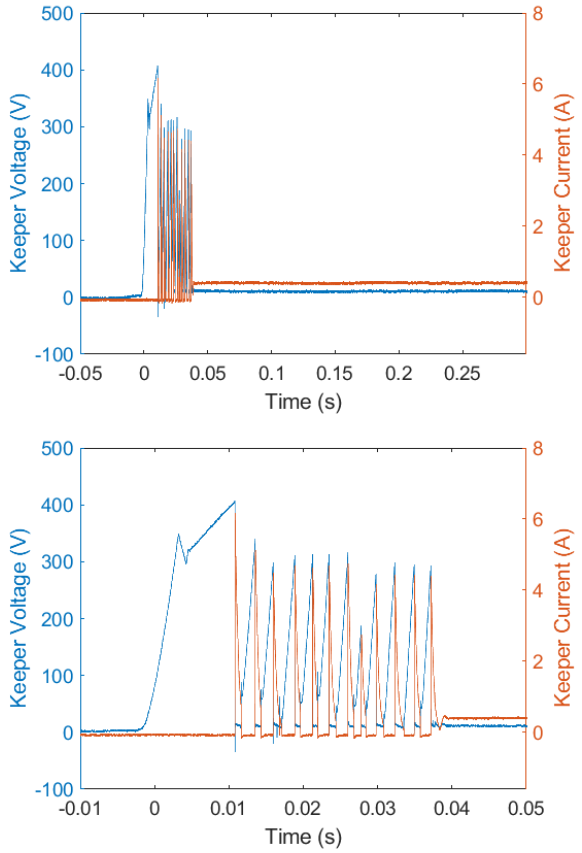

Figure 7: A sample MaSMi-EM heaterless cathode ignition from the LIF campaign that followed the 7205-hour wear test. Both panels display the same startup data, with a zoomed-in timescale shown in the bottom panel.

In order to characterize the ignition behavior of a cathode that had been operated for many thousands of hours in a thruster, high-speed data electrical telemetry were captured for a number of ignitions during the LIF campaign that followed the 7205-hour MaSMi-EM wear test. One example is shown in Fig. 7. 40 sccm xenon flow was supplied to the cathode, and ignition was triggered with the keeper power supply set to 1000 V voltage limit and 0.5 A current limit. The figure shows that the initial breakdown occurred at a keeper voltage around 400 V (the brief dip during the initial keeper voltage ramp-up is a power supply behavior unrelated to the cathode). Twelve consecutive ignition strikes occurred before the cathode transitioned into a stable 0.5 A keeper discharge within <50 ms; for heaterless cathodes, it is typical for multiple Paschen breakdown events to be necessary in order to heat the insert (emitter) to a sufficient temperature for self-sustaining thermionic emission. At the time of the ignition shown, this cathode had been running in the thruster for ~ 6300 h; the cathode that started the LDWT had to be replaced after it was damaged during thruster disassembly as part of an investigation of an unrelated material time-at-temperature anomaly early in the wear test.[11]

Cathode Life Modeling

In addition to evaporation of the LaB_6 emitter, hollow cathode life can be limited by radial erosion of the cathode orifice and axial erosion of the keeper electrode face. Significant examples of these two erosion phenomena were observed in the neutralizer[34] and discharge[24] cathodes, respectively, during life testing of the NSTAR ion thruster.[35] The physical processes driving the erosion were elucidated largely through the 2D cathode plasma modeling code OrCa2D,[36] which has since been used to simulate erosion over life for a number of cathodes designed for operation from 1 A to >100 A discharge current. The code solves the plasma fluid conservation equations in both the high-density insert-region and in the cathode plume, and it incorporates a first-principles model of anomalous electron resistivity arising from ion acoustic turbulence in the cathode plume.[37]

While the 13000-hour cathode wear test demonstrated long life of the MaSMi-EM cathode with minimal erosion at 4 A discharge current, the erosion processes do not scale proportionally with current. To ensure that the cathode had sufficient life at lower current throttle points, OrCa2D simulations were run at 4 A, 2 A, 1.6 A, and 1 A. The simulations were validated against measurements of the discharge voltage and keeper floating voltage from performance characterizations carried out at intervals during the cathode wear test.[10] Figure 8 shows examples of electron density contours calculated in

the simulations at 4 A and 1 A. The cathode interior is on the lower left of each figure, with the density peak localized to the emitter region at 1 A and extending into the cathode and keeper orifices at 4 A.

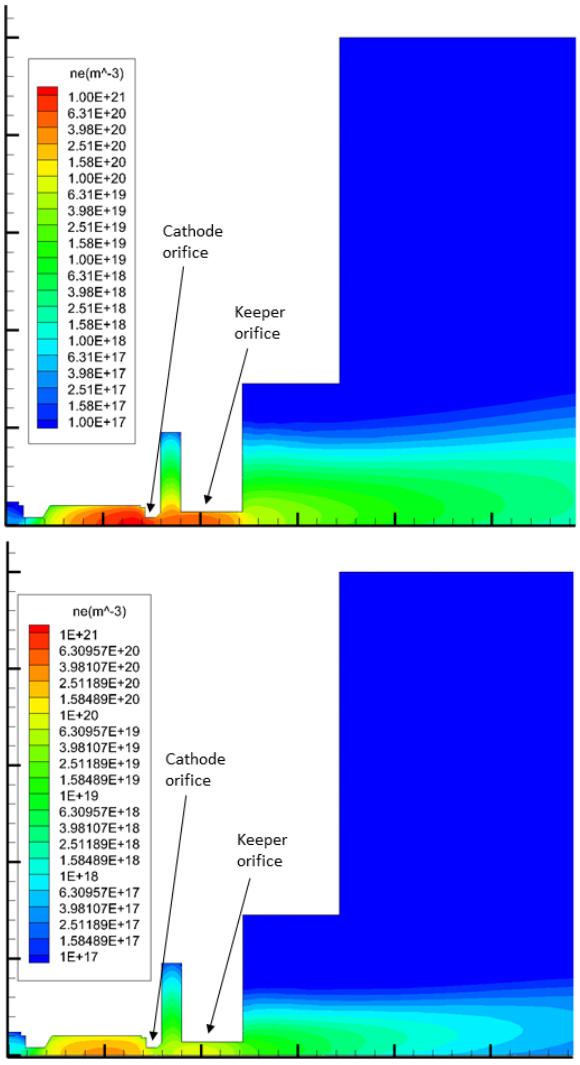

Figure 8: Time-averaged electron density contours from OrCa2D simulations of the MaSMi-EM hollow cathode operating at 4 A (top) and 1 A (bottom) discharge currents.

Table 1 presents key results from the cathode simulations. While emitter temperatures have been measured in some larger cathodes,[38] this has not been practical in the miniature MaSMi cathode, so an iterative process was used to determine the temperature that gave the correct discharge current in the simulations while also matching the measured electrical telemetry. The predicted erosion rates of the keeper face and cathode orifice barrel both increased as the discharge current was lowered. Erosion of the graphite keeper remained negligible at all operating conditions ($\ll 1$ μm/kh). The erosion rate of the tungsten plate orifice was also low, but it could become important relative to the initial diameter of the orifice during very long-duration operation at low discharge currents.

Table 1: OrCa2D cathode life simulation results. The emitter temperature listed is at the hottest location, and the erosion rates are listed in μm/kh.

I_d (A)	4.0	2.0	1.6	1.0
$T_{emitter}$ (C)	1410	1310	1290	1240
Orifice Erosion	2.03	1.89	3.25	6.67
Keeper Erosion	0.001	0.005	0.013	0.160

RELIABILITY ANALYSIS

Micrometeoroid and Orbital Debris Analysis

Satellite components such as Hall thrusters that are mounted to the exterior of a spacecraft are at risk of damage from impacts by micrometeoroids and orbital debris (MMOD). MaSMi-EM/Halo12 was analyzed to predict the failure rate due to these impacts for missions confined to the inner solar system (heliocentric distance <2 AU). Inspection of the thruster design revealed that the primary at-risk component was the outer coil, which resides beneath a stainless steel screen that is partially exposed by cutouts in the housing (outer magnetic core), as shown in Fig. 9. All other areas of the thruster have sufficient wall thickness to demonstrate negligible MMOD damage risk without detailed calculations.

The MMOD penetration analysis was carried out using the Bumper 3 code,[39] which was originally developed by the Hypervelocity Impact Technology (HVIT) group at NASA Johnson Space Center (JSC) and has been used to analyze the International Space Station,[40] the Space Shuttle, the James Webb Space Telescope, and many other NASA and commercial satellites. The code uses ballistic limit equations, derived from a combination of hypervelocity impact tests[41] and numerical simulations, to calculate penetration rates for spacecraft surfaces based on the assumed material properties, geometry, and MMOD environment. The calculations used Meteoroid Engineering Model 3 (MEM3),[42] which is NASA's most current and accurate model of the micrometeoroid environment.

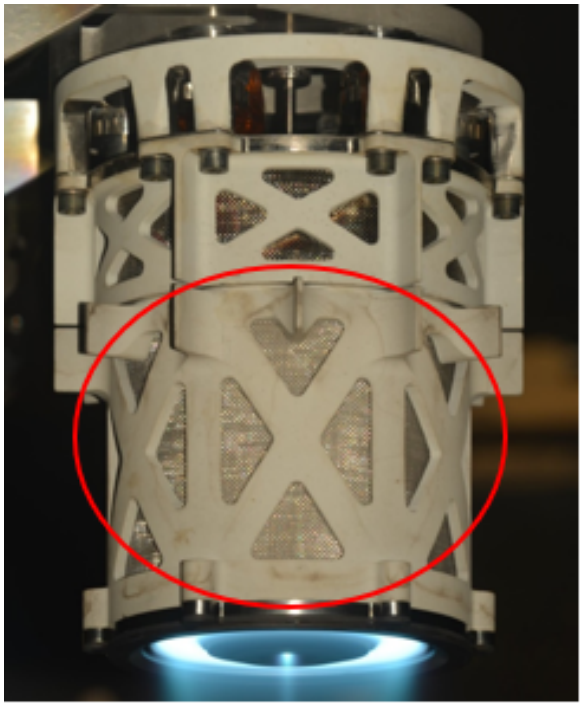

Figure 9: Area of interest for micrometeoroid and orbital debris analysis.

Coil failure was defined as a particle penetrating through half of the coil wire thickness, which could cause the coil wire to fully break during subsequent thermal cycling. The coil wire, insulation, and potting compound materials did not have ballistic limit equations available in Bumper 3, so they were approximated as a single layer of stainless steel with equivalent total mass per unit impact area. An aluminum equivalent layer was also analyzed and was found to be 6 times less conservative in terms of the MMOD penetration rate. While stainless steel may not be the most conservative possible material choice, the single-layer approximation also adds conservatism, since particles passing through multiple material interfaces would be slowed by reflections and shock waves.

Figure 10 shows the calculated coil wire penetration rate as a function of allowed penetration depth for particles incident from 6 directions that define the face of a cube (to account for anisotropy in the micrometeoroid flux). The orientation with the greatest number of perforations was used in the final calculation for conservatism. In a typical thruster mounting configuration, the spacecraft body shields approximately half of the solid angle from which micrometeoroids may be incident. Using the results from Fig. 10 along with the exposed coil area and the allowed penetration depth, and accounting for this shielding, the predicted failure rate in flight was 3.5×10^{-4} failures/year $= 0.041$ failures/10^6 hours.

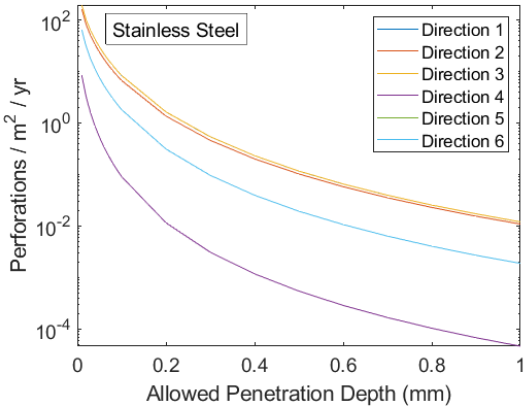

Figure 10: Bumper 3 prediction of the micrometeoroid penetration rate for stainless steel in the MEM3 environment.

Random Failure Rate Calculation

The MMOD failure rate was folded into a more comprehensive calculation of the overall in-flight random failure rate for the thruster. A standard reliability analysis framework was followed, as outlined in the Military Handbook for Reliability Prediction of Electronic Equipment (MIL-HDBK-217F).[43] The analysis included all electronic components in the thruster such as coils and connectors, as well as mechanical joints such as electron-beam welds, spot welds, and brazes. Base failure rates λ_b from MIL-HDBK-217F were used, with extra conservatism added where appropriate (for example, the random failure rate for spot welds was assumed to be 1000x higher than the handbook's rate for welded electrical connections). Each base rate was modified by π factors[43] to determine the adjusted failure rate:

$$\lambda_p = \lambda_b n \pi_E \pi_T \pi_A \pi_K. \quad (2)$$

Here n is the quantity of a given component in the thruster, π_E is an environmental factor (equal to 0.5 for space flight), π_T is a temperature factor, π_A is an application factor (equal to 1 for operation and 0.1 for dormant non-operation except in the case of welds, brazes and other connections), and π_K is a mating/unmating factor for connectors.

For redundant components, the number of surviving instances required to maintain in-spec thruster operation was conservatively estimated. The mission survival probability P_S for the redundant component group, defined as the probability that fewer than m out of N redundant components

fail, is:

$$P_S = \sum_{k=0}^{m-1} \frac{N!}{k!\,(N-k)!} P_{S1}^{N-k} \left(1 - P_{S1}\right)^k , \tag{3}$$

where P_{S1} is the probability that any one component survives. The overall survival probability is related to the effective failure rate for the redundant group by:

$$\lambda_{p,eff.} = -\frac{\ln\left(P_S\right)}{t} \tag{4}$$

where t is the mission duration that was assumed to calculate P_{S1}.

Combining the contributions from all components, the in-flight random failure rate for MaSMi-EM/Halo12 was calculated to be 4.3×10^{-4} failures/year = 0.049 failures/10^6 hours. Referring to the previous subsection, the dominant contribution came from MMOD-induced failures.

It is important to note that wear-out failure modes associated with extended thruster operation and with thermal cycling were explicitly excluded from the random failure rate calculation. The failure rate distributions (mean lifetime and spread) for these thruster-specific failure modes are not known,[21] inhibiting inclusion in a standard reliability analysis framework. As is typical for Hall thrusters, the MaSMi-EM/Halo12 qualification program will rely on testing, engineering analysis (e.g., structural and thermal), and plasma modeling of erosion processes to demonstrate sufficient life margin for these failure modes. The reliability analysis framework described here essentially measures the complexity of the thruster design, providing an estimate of the remaining failure probability after targeted qualification testing and analysis has demonstrated that the design is fundamentally sound.

CONCLUSION

Recent progress in the flight qualification of the MaSMi-EM/Halo12 Hall thruster has been summarized. The MaSMi-EM Long Duration Wear Test, which previously achieved 100 kg of xenon propellant throughput, will be extended to further qualify the service life capability of thruster. Ongoing investigations including LIF measurements, magnetic field mapping, and physics-based modeling seek to understand the root cause of asymmetric front pole erosion observed in the wear test thruster, raising the possibility that future units could have even longer life if the issue can be eliminated. Cathode life modeling using the OrCa2D code showed that orifice plate and keeper face erosion are not expected to be important life limiting factors for realistic mission throttle profiles. Heaterless cathode ignitions have been studied both in the wear thruster and in a stand-alone cathode test fixture, demonstrating reliable startups late in the thruster's life. Finally, quantitative reliability analysis was carried out to calculate the thruster's random failure rate in flight, including the contribution from micrometeoroid impacts.

ACKNOWLEDGMENTS

This research was carried out at the Jet Propulsion Laboratory (JPL), California Institute of Technology, under a contract with the National Aeronautics and Space Administration (80NM0018D0004). The authors thank Nowell Niblett and Mario Delgado for their critical assistance with the test setups and vacuum facility maintenance. We also acknowledge valuable program management contributions from Bob Cicone and Jeff Greteman at Exoterra.

References

[1] R. W. Conversano, D. M. Goebel, R. R. Hofer, T. S. Matlock, and R. E. Wirz. Development and initial testing of a magnetically shielded miniature Hall thruster. *IEEE Trans. Plasma Sci.*, 43(1):103–117, 2015.

[2] R. W. Conversano, D. M. Goebel, R. R. Hofer, I. G. Mikellides, and R. E. Wirz. Performance analysis of a low-power magnetically shielded Hall thruster: Experiments. *J. Propul. Power*, 33(4):975–983, 2017.

[3] R. W. Conversano, D. M. Goebel, I. G. Mikellides, R. R. Hofer, and R. E. Wirz. Performance analysis of a low-power magnetically shielded Hall thruster: Computational modeling. *J. Propul. Power*, 33(4):992–1001, 2017.

[4] A. Lopez Ortega, I. G. Mikellides, R. W. Conversano, R. B. Lobbia, and V. H. Chaplin. Plasma simulations for the assessment of pole erosion in the Magnetically Shielded Miniature Hall Thruster (MaSMi). In *36th International Electric Propulsion Conference*, Vienna, Austria, September 2019. IEPC-2019-281.

[5] R. B. Lobbia, et al. Pole erosion measurements for the development model of the Magnetically Shielded Miniature Hall Thruster (MaSMi-DM). In *36th International Electric Propulsion*

Conference, Vienna, Austria, September 2019. IEPC-2019-298.

[6] V. H. Chaplin, R. W. Conversano, A. Lopez Ortega, I. G. Mikellides, R. B. Lobbia, and R. R. Hofer. Ion velocity measurements in the Magnetically Shielded Miniature Hall Thruster (MaSMi) using laser-induced fluorescence. In *36th International Electric Propulsion Conference*, Vienna, Austria, September 2019. IEPC-2019-531.

[7] R. W. Conversano, R. B. Lobbia, T. V. Kerber, K. C. Tilley, D. M. Goebel, and S. W. Reilly. Performance characterization of a low-power magnetically shielded Hall thruster with an internally-mounted hollow cathode. *Plasma Sources Sci. Technol.*, 28:105011, 2019.

[8] R. W. Conversano, A. Barchowsky, R. B. Lobbia, V. H. Chaplin, A. Lopez Ortega, J. A. Loveland, A. D. Lui, G. Becatti, S. W. Reilly, D. M. Goebel, J. S. Snyder, R. R. Hofer, T. M. Randolph, I. G. Mikellides, V. Vorperian, , G. A. Carr, J. Rapinchuk, C. Y. Villalpando, and D. Grebow. Overview of the Ascendant Sub-kW Transcelestial Electric Propulsion System. In *36th International Electric Propulsion Conference*, Vienna, Austria, September 2019. IEPC-2019-282.

[9] R. W. Conversano, S. W. Reilly, T. V. Kerber, J. W. Brooks, and D. M. Goebel. Development of and acceptance test preparations for the thruster component of the Ascendant Sub-kW Transcelestial Electric Propulsion System (ASTRAEUS). In *36th International Electric Propulsion Conference*, Vienna, Austria, September 2019. IEPC-2019-283.

[10] R. W. Conversano, G. Becatti, D. M. Goebel, and V. H. Chaplin. Demonstration of 13,011-h of operation of a proto-flight compact heaterless lanthanum hexaboride hollow cathode. *Acta Astronautica*, 197:53–59, 2022.

[11] R. W. Conversano, R. B. Lobbia, S. M. Arestie, A. Lopez Ortega, V. H. Chaplin, S. W. Reilly, and D. M. Goebel. Demonstration of one hundred kilogram xenon throughput by a low-power Hall thruster. *J. Prop. Power*, 39(2):217–231, 2023.

[12] I. G. Mikellides, I. Katz, R. R. Hofer, and D. M. Goebel. Magnetic shielding of walls from the unmagnetized ion beam in a Hall thruster. *Appl. Phys. Lett.*, 102:023509, 2013.

[13] R. R. Hofer, D. M. Goebel, I. G. Mikellides, and I. Katz. Magnetic shielding of a laboratory Hall thruster. II. Experiments. *J. Appl. Phys.*, 115:043304, 2014.

[14] L. Grimaud and S. Mazouffre. Ion behavior in low-power magnetically shielded and unshielded Hall thrusters. *Plasma Sources Sci. Technol.*, 26:055020, 2017.

[15] L. M. Lidsky, S. D. Rothleder, D. J. Rose, S. Yoshikawa, C. Michelson, and R. J. Mackin, Jr. Highly ionized hollow cathode discharge. *J. Appl. Phys.*, 33(8):2490–2497, 1962.

[16] D. Lev and L. Appel. Heaterless hollow cathode technology - a critical review. In *Space Propulsion Conference*, Rome, Italy, May 2016.

[17] D. R. Lev, I. G. Mikellides, D. Pedrini, D. M. Goebel, B. A. Jorns, and M. S. McDonald. Recent progress in research and development of hollow cathodes for electric propulsion. *Rev. Mod. Phys.*, 3:6, 2019.

[18] Z.-X. Ning, H.-G. Zhang, X.-M. Zhu, L. Ouyang, X.-Y. Liu, B.-H. Jiang, and D.-R. Yu. 10000-ignition cycle investigation of a LaB_6 hollow cathode for a 3–5-kilowatt Hall thruster. *J. Prop. Power*, 35(1):87–92, 2019.

[19] G. Becatti, R. W. Conversano, and D. M. Goebel. Demonstration of 25,000 ignitions on a proto-flight compact heaterless lanthanum hexaboride hollow cathode. *Acta Astronautica*, 178:181–191, 2021.

[20] R. R. Hofer and J. R. Anderson. Finite pressure effects in magnetically shielded Hall thrusters. In *50th AIAA/ASME/SAE/ASEE Joint Propulsion Conference*, Cleveland, OH, July 2014. AIAA-2014-3709.

[21] J. E. Polk and J. R. Brophy. Life qualification of Hall thrusters by analysis and test. In *Space Propulsion 2018 Conference*, Seville, Spain, May 2018. Paper 00547.

[22] R. W. Conversano, A. Barchowsky, V. Vorperian, V. H. Chaplin, G. Becatti, G. A. Carr, C. B. Stell, J. A. Loveland, and D. M. Goebel. Cathode & electromagnet qualification status and power processing unit development update for the Ascendant Sub-kW Transcelestial Electric Propulsion System. In *34th Annual Small Satellite Conference*, Logan, UT, 2020. SSC20-VI-10.

[23] M. A. Frerking and P. M. Beauchamp. JPL technology readiness assessment guideline. In *IEEE Aerospace Conference*, Big Sky, MT, March 2016.

[24] I. G. Mikellides and I. Katz. Wear mechanisms in electron sources for ion propulsion II: Discharge hollow cathode. *J. Propul. Power*, 24(4):866–879, 2008.

[25] S. Mazouffre. Laser-induced fluorescence diagnostics of the cross-field discharge of Hall thrusters. *Plasma Sources Sci. Technol.*, 22:013001, 2013.

[26] V. H. Chaplin, B. A. Jorns, A. Lopez Ortega, I. G. Mikellides, R. W. Conversano, R. B. Lobbia, and R. R. Hofer. Laser-induced fluorescence measurements of acceleration zone scaling in the 12.5 kW HERMeS Hall thruster. *J. Appl. Phys.*, 124:183302, 2018.

[27] W. Huang and H. Kamhawi. Counterstreaming ions at the inner pole of a magnetically shielded Hall thruster. *J. Appl. Phys.*, 129:043305, 2021.

[28] I. G. Mikellides and I. Katz. Numerical simulations of Hall-effect plasma accelerators on a magnetic-field-aligned-mesh. *Phys. Rev. E*, 86:046703, 2012.

[29] A. Lopez Ortega, I. G. Mikellides, M. J. Sekerak, and B. A. Jorns. Plasma simulations in 2-D (r-z) geometry for the assessment of pole erosion in a magnetically shielded Hall thruster. *J. Appl. Phys.*, 125:033302, 2019.

[30] N. B. Meezan, W. A. Hargus, and M. A. Cappelli. Anomalous electron mobility in a coaxial Hall discharge plasma. *Phys. Rev. E*, 63:026410, 2001.

[31] J. C. Adam, A. Héron, and G. Laval. Study of stationary plasma thrusters using two-dimensional fully kinetic simulations. *Phys. Plasmas*, 11:295, 2004.

[32] I. G. Mikellides and A. Lopez Ortega. Challenges in the development and verification of first-principles models in Hall effect thruster simulations that are based on anomalous resistivity and generalized Ohm's law. *Plasma Sources Sci. Technol.*, 28:014003, 2019.

[33] S. E. Cusson, E. T. Dale, B. A. Jorns, and A. D. Gallimore. Acceleration region dynamics in a magnetically shielded Hall thruster. *Phys. Plasmas*, 26:023506, 2019.

[34] I. G. Mikellides and I. Katz. Wear mechanisms in electron sources for ion propulsion I: Neutralizer hollow cathode. *J. Propul. Power*, 24(4):855–865, 2008.

[35] A. Sengupta, J. R. Brophy, and K. D. Goodfellow. Status of the extended life test of the Deep Space 1 flight spare ion engine after 30,352 hours of operation. In *39th AIAA/ASME/SAE/ASEE Joint Propulsion Conference and Exhibit*, Huntsville, AL, July 20–23 2003. AIAA 2003-4558.

[36] I. G. Mikellides, I. Katz, D. M. Goebel, and K. K. Jameson. Evidence of nonclassical plasma transport in hollow cathodes for electric propulsion. *J. Appl. Phys.*, 101:063301, 2007.

[37] A. Lopez Ortega, B. A. Jorns, and I. G. Mikellides. Hollow cathode simulations with a first-principles model of ion-acoustic anomalous resistivity. *J. Prop. Power*, 34(4):1026–1038, 2018.

[38] P. P. Guerrero Vela, J. E. Polk, M. H. Richter, and A. Lopez Ortega. Dynamic thermal behavior of polycrystalline lab_6 hollow cathodes. *J. Appl. Phys.*, 130:083303, 2021.

[39] D. M. Lear, E. L. Christiansen, and J. L. Hyde. Bumper: A tool for analyzing spacecraft micrometeoroid and orbital debris risk. In *1st International Orbital Debris Conference (IOC)*, Sugar Land, TX, December 2019.

[40] J. L. Hyde, E. L. Christiansen, D. M. Lear, K. Nagy, and E. L. Berger. Surveys of returned iss hardware for MMOD impacts. In *Proc. 7th European Conference on Space Debris*, Darmstadt, Germany, April 18–21 2017.

[41] B. G. Cour-Palais. Hypervelocity impact in metals, glass, and composites. *Int. J. Impact Engng.*, 5:221–237, 1987.

[42] A. V. Moorhead. NASA meteoroid engineering model (MEM) version 3. Technical Report NASA/TM–2020–220555, NASA Marshall Space Flight Center, Huntsville, AL, 2020.

[43] Reliability prediction of electronic equipment. Technical Report MIL-HDBK-217F, U.S. Department of Defense, December 1991.